Discover Materials

RESEARCH Open Access

Modeling of deformation twinning in BCC metals via quantum annealing

Lara Caroline Pereira dos Santos[1], Antje Dollmann[2,3], Christian Greiner[2,3], Daniel Grüner[1], Yann Le Bouar[4] and Robert Spatschek[1,5*]

*Correspondence:
Robert Spatschek
r.spatschek@fz-juelich.de
[1]Institute of Energy Materials and Devices (IMD-1), Forschungszentrum Jülich GmbH, Jülich 52425, Germany
[2]Institute for Applied Materials (IAM), Karlsruhe Institute of Technology (KIT), Kaiserstraße 12, Karlsruhe 76131, Germany
[3]IAM-ZM MicroTribology Center (μTC), Straße am Forum 5, Karlsruhe 76131, Germany
[4]Laboratoire d'Etude des Microstructures, Université Paris-Saclay, ONERA, CNRS, Châtillon 92320, France
[5]JARA-ENERGY, Jülich 52425, Germany

Abstract

The accurate prediction of microstructures under mechanical stresses is crucial for understanding materials behavior, especially in body-centered cubic (bcc) metals where the deformation phenomena remain elusive. In this work, we introduce a continuum framework, linked to crystallographic considerations and atomistic simulations, to model deformation twinning in bcc systems using quantum annealing. This requires formulation of the problem in terms of the global minimization of an Ising Hamiltonian, with coefficients reflecting the elastic interactions between discretization domains. We perform qualitative comparisons with atomistic simulations and quantitative benchmarking against analytical solutions in well-defined setups, and demonstrate the scalability to larger, polycrystalline specimens, where atomistic methods become prohibitive due to high computational costs, outputting qualitatively similar pictures as experiments. The scale-bridging, quantum annealing based model provides an efficient and novel computational framework for determining equilibrium microstructures in single crystals and polycrystals under mechanical stresses, with emphasis on systems where twinning is a dominant deformation mechanism.

1 Introduction

Understanding and simulating deformation mechanisms and microstructure formation are central for tailoring materials with desired mechanical properties. Traditionally, models have relied on classical approaches across multiple scales: starting at defect formation using electronic structure calculations (e.g., [1, 2]), moving on to different types of defects and deformation mechanisms on atomistic scales via Molecular Dynamics, Molecular Statics or Monte Carlo approaches (e.g., [3, 4]), and finishing with descriptions at the continuum using finite element or volume elements (e.g., [5]). With the advent of quantum computing, a key question that arises is whether this new technology can contribute to simulating materials mechanics already today, potentially outperforming classical modeling methods in the future. So far, applications in this pioneering field are rare, mainly due to hardware constraints, such as the number of qubits and the presence of (quantum) noise. However, remarkable contributions from quantum computing

to materials mechanics and materials science are already possible [6–16]. These innovations have the potential to support and complement existing modeling approaches and may eventually even surpass them. Based on preliminary work on the formation of martensite [6, 7] and microstructures in ceramic solid electrolytes [8] within a continuum mechanics framework, we demonstrate here the use of quantum annealing (QA), a specific branch of quantum computing, on the prediction of deformation twinning in bcc metals.

Body-centered cubic (bcc) metals primarily deform either by dislocation motion or by deformation twinning. Both deformation mechanisms are relevant and this topic has remained as a widely studied field persisting until these days [3, 4, 17–23]. In close-packed metallic structures, deformation twins are well understood and have been extensively used to design materials with exceptional mechanical properties [24–26]. However, in bcc metals, deformation twinning endures as an elusive and intricate phenomenon [19, 23]. Achieving a deeper insight into the twinning mechanisms in bcc structures, as well as simulating it on larger scales, could open up new possibilities to enhance these materials' performance, applicability and understanding.

Not only deformation twins, but also growth and annealing twins can occur within metals [23, 27]. Growth twins are formed far from equilibrium mostly during initial crystal growth [23]. Annealing twins appear during recrystallization of previously deformed metals, and there is no deformation associated with their formation. Instead, they form as a result of minimization of interfacial energy and grow diffusionally [28, 29]. On the other hand, deformation twins minimize elastic strain energy and there is a clear deformation associated to their formation. Deformation twins occur as a result of a large deformation of a single grain and have a lenticular morphology, since the small thickness to length ratio minimizes the long-range elastic strain [28].

Deformation twinning in bcc metals occurs by shearing the crystal on $\{112\}$ planes along the $\langle 111 \rangle$ directions, and it is associated with a twinning/anti-twinning anisotropy [3]. In bcc transition metals, such as α-iron and niobium, deformation twinning has been studied frequently [18, 19, 30–33]. However, in bcc alkali metals, such as lithium and sodium, the deformation behavior is still largely under-reported due to the difficult handling. Nevertheless, with the advance of solid-state batteries and the prospect of using metal anodes, specific knowledge about these materials became a necessity [34–36]. While it is reasonable to infer that the alkali metals exhibit similar characteristics as the other bcc metals, direct confirmation is necessary to assert it definitively. Recently, Molecular Statics simulations of all bcc metals showed that deformation twinning in the alkali metals indeed occurs only on $\{112\}$ planes, but with a lower likelihood of anti-twin formation compared to transition metals, due to the stronger asymmetry of energy barriers [3].

Generally, atomistic simulations can handle only a relatively small number of atoms and single crystals setups, since the simulation of large-scale and polycrystalline samples is computationally demanding via these methods. To address twinning in polycrystalline materials, continuum-based modeling approaches (see, e.g., [5]) and phase-field models (see, e.g., [37]) have been developed. Despite their differences in scale and methodology, these approaches have a common goal to predict the dynamics of the system, either based on interatomic potentials for the atomistic descriptions or crystal plasticity slip laws for the continuum models [3, 5]. In all these cases, which are based on

time dependent formulation, a relaxation to equilibrated twin structures may require extended simulation times, which typically exceed the capabilities of atomistic and possibly also continuum simulations. Moreover, phase field approaches follow an evolution dynamics of the type $\dot{\phi} \sim -\delta F/\delta\phi$, where ϕ can be used as order parameter to identify twinned regions, and the free energy F includes in particular the elastic energy. As phase field methods act as local energy minimization approaches during time evolution, $\dot{F} < 0$, they can get stuck in local minima (unless fluctuations are considered), which makes the determination of the absolute energy minimum difficult. Therefore, phase field should mainly be considered as an approach to predict the dynamics and evolution of transformations [38–42].

Here, we propose an alternative continuum picture, which directly determines the ground state configuration of the system under mechanical loads. Our approach minimizes the mechanical energy with respect to both the elastic degrees of freedom (i.e., displacements) and the evolving twinning microstructure, aligning with the fundamental definition of deformation twinning [28]. In this way, the description neither relies on empirical interatomic potentials nor on constitutive kinematic relations. Instead, it can be considered as a minimum model, based just on well established concepts of elasticity and crystallography. This energy based perspective complements considerations based on critical resolved shear stresses for the initiation of deformation twinning. In addition, twin interface energies are incorporated into the formulation. The elastic deformations are handled conventionally using classical computing. However, at each material point, an additional discrete variable is introduced to represent whether this region belongs to a twin or to the matrix. In this way, the direct determination of twin distributions becomes a hard combinatorial problem, as one needs to calculate the total energy of all possible arrangements of twins. This is the point at which quantum annealing gives a substantial benefit and efficiently optimizes the total energy of the system. The model is built on our previous work on shear transformations, where we have mapped the spatial arrangement of martensite variants to an Ising Hamiltonian, which is efficiently minimized using quantum annealing [6–8]. As the quantum annealing simulations are extremely fast, the ground state configuration is obtained very quickly, as compared to the aforementioned modeling approaches, offering new opportunities for simulating deformation twinning.

This article is structured as follows: To establish the new modeling paradigm, we firstly transfer the crystallographic aspects of twin formation in bcc metals to a continuum mechanics perspective in Sects. 2.1 and 2.2. In Sect. 2.3 the QA approach for modeling the deformation twinning is presented. Complementary Molecular Dynamics simulations (Sect. 2.4) serve as qualitative comparison for the model development. Next, in Sect. 3.1, we use layered planar interfaces representing twin boundaries to determine the preferred orientations of the deformation twins from a continuum perspective and ensure consistency with the crystallographic expectations. After that, in Sect. 3.2, the determination of the equilibrium twin structures via quantum annealing is introduced and demonstrated on single crystals for planar (112) twin formation under varying mechanical loads. Although the results confirm the Molecular Dynamics observations, still discrepancies remain, which are resolved by the consideration of interfacial energies in Sect, 3.3. With that, the transfer for the self-consistent equilibrium twin distributions

becomes feasible and is studied in Sect. 3.4 for polycrystals, to demonstrate the capabilities and limitations of the novel quantum computing-based approach.

2 Methods

2.1 Crystallography

According to the crystallographic definition [43], a twin is an intergrowth of two or more individuals of the same crystal species with a well-defined crystallographic orientation relationship. This orientation relationship is given by the twin law, which comprises the set of symmetry operations and elements that transform the lattice of one individual into the lattice of the other one. The individuals that form the twin are called twin components or domains, while their individual orientation corresponds to the respective orientation states. The contact plane between two individuals is called twin interface or domain boundary. Although the term domain is commonly used describing twins composed of lamellar twin components, we rather use the term twin component in order to avoid confusion with the discretization domains used for the QA description. It should be noted, however, that here a discretization domain corresponds to the smallest possible twin component. Furthermore, in the literature on metallurgy and especially in studies of deformation twinning, the term "twin" is ascribed to twin components formed by deformation twinning, while the part of the grain that remains in its original orientation state is designated "matrix", see the examples presented in [23]. In this work we refer to twin components characterized by their respective orientation state — transformed or original —, as the size or volume fraction of the transformed twin components may exceed that of twin components with the original orientation state.

In the case of the bcc crystal structure, the commonly observed twin interfaces are the $\{112\}$ planes [3, 23], and the orientation states of adjacent twin components are related by a reflection on this plane. The corresponding twin law is the so-called *spinel law*, which is associated with a $\Sigma = 3$ coincidence site lattice; i.e., the twin interfaces are $\Sigma 3$ boundaries.

To express the transformation strain through the twinning, we consider twinning on a (112) plane specifically and introduce a local coordinate system spanned by orthogonal unit vectors $\hat{x}' \parallel [\bar{1}\bar{1}1]$, $\hat{y}' \parallel [1\bar{1}0]$ and $\hat{z}' \parallel [112]$. Here, $\hat{y}'$ is the in plane direction of translational invariance in the sense of a plane strain description, while $\hat{x}'$ is the twinning direction and $\hat{z}'$ the twin interface normal, as indicated in Fig. 1. All Miller indices designating crystallographic planes or directions refer to the original orientation state unless stated otherwise. The bcc crystal structure can be built by stacking layers of atoms situated on (112) planes (dashed lines in Fig. 1). Each layer is shifted relative to the previous one by $a/(2\sqrt{3})$ along $[\bar{1}\bar{1}1]$, with a being the lattice constant. The stacking sequence repeats every six layers (*ABCDEF* stacking sequence, note that the atoms on every second layer are located above/below the projection plane). Twinning can then be described by additional shifts of the (112) planes by $a/(2\sqrt{3})$ for the first layer (green arrow), $2 \times a/(2\sqrt{3})$ for the second layer (twice the green arrow), etc., such that the stacking sequence is reversed (into *FEDCBA*) and the upper part of the crystal becomes mirror symmetric to the lower one. Anti-twinning, which will not be considered in this study, could be described by additional shifts of the (112) planes by $-a/\sqrt{3}$ for the first layer, $-2 \times a/\sqrt{3}$ for the second layer, etc., resulting in the same atomic arrangement as twinning. Deformation twinning of the crystal can therefore be understood as a shear of the

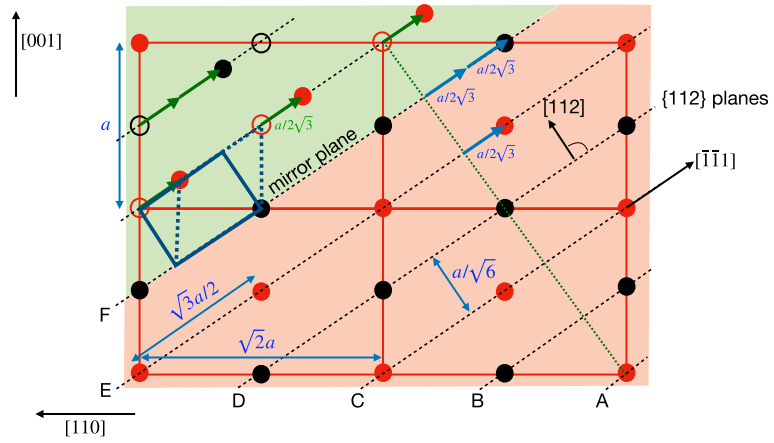

Fig. 1 Projection of the crystal structure of a twinned bcc crystal with lattice constant a onto the $(1\bar{1}0)$ plane. Atoms, which belong to the same plane in the projection view are coded with the same colour (black or red). In the green region, where the twinning takes place through the collective movement of partial dislocations, the atoms are moved from the parent crystal positions (open spheres) to new locations (solid spheres). The red region corresponds to the original lattice (original orientation state), whereas the green region goes through the shear transformation (resulting in the transformed orientation state). The twin interface is a (112) plane, which is at the same time a twin mirror plane. The blue solid rectangle is sheared to the dashed one upon twinning. *ABCDEF* refers to the stacking sequence, which is reversed by the twin transformation.

original lattice, as illustrated by the transition from the solid to the dashed blue rectangle in Fig. 1. With the lateral shift by $\Delta u_{x'} = a/2\sqrt{3}$ per interplanar distance $\Delta z' = a/\sqrt{6}$, the shear strain therefore becomes in the rotated reference frame

$$\epsilon^{\text{twin}}_{x'z'} = \frac{1}{2}\left(\frac{\partial u_{x'}}{\partial z'} + \frac{\partial u_{z'}}{\partial x'}\right) = \frac{1}{2\sqrt{2}}. \tag{1}$$

For an orthonormal, right handed basis set $B' = \{\hat{x}', \hat{y}', \hat{z}'\}$, the symmetric twin eigenstrain tensor therefore becomes [44]

$$\epsilon^{\text{twin}'} = \begin{pmatrix} 0 & 0 & 1/(2\sqrt{2}) \\ 0 & 0 & 0 \\ 1/(2\sqrt{2}) & 0 & 0 \end{pmatrix} = {}_{B'}[\epsilon^{\text{twin}}]_{B'}. \tag{2}$$

In particular, the direction $\hat{y}'$ remains invariant under the transformation.

Whereas a local analysis of the twinning process is easier in this rotated reference frame, for an inspection from the laboratory system a transformation to a basis set $B = \{\hat{x}, \hat{y}, \hat{z}\}$ is desirable, using (normalized) unit vectors $\hat{x} \parallel [\bar{1}\bar{1}0]$, $\hat{y} \parallel \hat{y}' \parallel [1\bar{1}0]$ and $\hat{z} \parallel [001]$. We note that we keep the $45°$ rotation in the xy plane relative to the conventional basis vectors, as this allows to keep a reduction to a two-dimensional (xz) plane strain description.

With these definitions, we have

$$\hat{x}' = \frac{1}{\sqrt{3}}\begin{pmatrix} -1 \\ -1 \\ 1 \end{pmatrix} = \sqrt{\frac{2}{3}}\hat{x} + \frac{1}{\sqrt{3}}\hat{z}, \tag{3}$$

$$\hat{z}' = \frac{1}{\sqrt{6}}\begin{pmatrix} 1 \\ 1 \\ 2 \end{pmatrix} = -\frac{1}{\sqrt{3}}\hat{x} + \sqrt{\frac{2}{3}}\hat{z}. \tag{4}$$

Therefore, the coordinate transformation matrix from basis set B to B' is given by

$$ {}_B[\mathrm{id}]_{B'} = \begin{pmatrix} \sqrt{2/3} & 0 & -\frac{1}{\sqrt{3}} \\ 0 & 1 & 0 \\ \frac{1}{\sqrt{3}} & 0 & \sqrt{2/3} \end{pmatrix}, \tag{5} $$

which maps the unit vectors from set B to B'. In the laboratory frame B the twin transformation strain tensor becomes

$$ {}_B[\epsilon^{\mathrm{twin}}]_B = {}_B[\mathrm{id}]_{B'}\, {}_{B'}[\epsilon^{\mathrm{twin}}]_{B'}\, {}_{B'}[\mathrm{id}]_B{}^{\dagger} \tag{6} $$

$$ = \begin{pmatrix} -1/3 & 0 & 1/(6\sqrt{2}) \\ 0 & 0 & 0 \\ 1/(6\sqrt{2}) & 0 & 1/3 \end{pmatrix}. \tag{7} $$

We focus here only this single bcc twinning system, but the generalization to more systems is possible.

2.2 Elasticity

We pursue a continuum description of deformation twin formation, to extend atomistic descriptions to larger scales using well established concepts only. The description is based on linear elasticity. For the purpose of illustration, we use a two-dimensional plane setup. This is legitimate if the out-of-plane direction coincides with the $\hat{y}'$ direction, as according to the transformation strain no deformation is induced in this direction for suitable boundary conditions. As simplification we use isotropic elasticity to reduce the number of elastic constants, although an extension to anisotropic descriptions is possible. In the isotropic limit, the Young's modulus scales out of the description, and only a weak dependence on the Poisson ratio remains, which it is not critical here. We point out that the strongest source of the anisotropy is the transformation strain (7) which is significantly larger than the anisotropy of the elastic constants of bcc metals.

The formation of twins is expressed through a local stress free strain or eigenstrain, ϵ^{twin}. From point of view of continuum elasticity, the microstructure is therefore defined by the knowledge of whether at any given location the crystal has undergone the shear transformation, leading to either an eigenstrain 0 (reference state indicating the original lattice orientation, i.e., a twin component with original orientation state) or a finite eigenstrain ϵ^{twin} (indicating the lattice after the shear transformation, i.e., a twin component with transformed orientation state). In conjunction with given boundary conditions, i.e., typically given strain or given stress, the problem is then well-posed in the framework of linear elasticity. We can in particular determine for a given microstructure the displacements, strains and stresses everywhere, as well as the stored elastic energy in the system.

For a given twin distribution inside the material, the elastic (free) energy is therefore given as [45]

$$ F_{\mathrm{el}} = \int dV \left(\frac{1}{2}\lambda(\epsilon_{kk} - \epsilon^{\mathrm{twin}}_{kk})^2 + \mu(\epsilon_{ik} - \epsilon^{\mathrm{twin}}_{ik})^2 \right), \tag{8} $$

where the integration is performed over the volume V of the sample; μ and λ are shear modulus and Lamé coefficient, respectively. The strains are derived from the displacement field components u_i, i.e.,

$$\epsilon_{ij} = \frac{1}{2}\left(\frac{\partial u_i}{\partial x_j} + \frac{\partial u_j}{\partial x_i}\right). \tag{9}$$

Mechanical equilibrium is obtained — for a given twin eigenstrain — through the minimization of the elastic energy with respect to displacements,

$$\frac{\delta F_{\mathrm{el}}}{\delta u_i} = 0, \tag{10}$$

which is performed here using Fourier transformation approaches (Khachaturyan method), assuming periodic boundary conditions, see [46] for details. In this way, the equilibrated elastic energy can be written as

$$F_{\mathrm{el}} = \frac{V}{2}\sum_{k\neq 0} B(\mathrm{n})|\hat{\theta}(\mathrm{k})|^2 \tag{11}$$

for a periodic system with vanishing average stress, where $\theta(\mathrm{r})$ is one in regions which have undergone the twinning transformation and zero everywhere else, and $\theta(\mathrm{k})$ is its Fourier transform. $B(\mathrm{n})$ with $\mathrm{n} = \mathrm{k}/k$ equals $B(\mathrm{n}) = \sigma_{ij}^{\mathrm{twin}}\epsilon_{ij}^{\mathrm{twin}} - n_i\sigma_{ij}^{\mathrm{twin}}\Omega_{jk}\sigma_{kl}^{\mathrm{twin}}n_l$ with $\sigma_{ij}^{\mathrm{twin}} = \lambda_{ijkl}\epsilon_{kl}^{\mathrm{twin}}$, allowing also for anisotropic stress-strain relations, $\sigma_{ij} = \lambda_{ijkl}(\epsilon_{kl} - \theta(\mathrm{r})\epsilon_{kl}^{\mathrm{twin}})$, beyond the isotropic case considered here for demonstration purposes. For a given mean strain $\langle\epsilon_{ij}\rangle$, an additional homogeneous contribution appears in the above expression for the energy [6–8].

Alternatively to the Fourier transformation approach, other solving procedures can be used like finite element methods, provided that the elastic energy is obtained with very high accuracy.

2.3 Quantum annealing

Quantum annealing (QA) belongs currently to the most advanced quantum computing approaches, which offers several thousands of qubits and couplers [47–51]. It can handle only specific classes of problems, namely binary quadratic optimization problems [52]. The basic concept of QA is the initialization of its qubits in well defined Hamiltonians, whose ground state is unique and known [53]. This Hamiltonian is then changed adiabatically at cryogenic temperatures to the desired, final problem Hamiltonian, ideally staying in the ground state throughout this transformation [53, 54] and therefore enabling an efficient global energy minimization.

We use the QA approach here in addition to the elastic solvers, which determine the equilibrium deformation state, for finding the energetically most favorable distribution of twins in the entire system of investigation. Therefore, we discretize the system into small domains. This tesselation can be done through a regular lattice as well as irregular regions, as discussed in [6]. We point out that the size of these domains does not have to coincide with an underlying grid or mesh size for solving the elastic problem. In fact, we usually use far less of these domains than grid points for the elastic solver. We assign to each of these domains a discrete indicator ("spin") s_i, where $s_i = -1$ corresponds to the original crystal (not twinned) and $s_i = +1$ to a domain after twinning, see Fig. 2 for an illustration. These spin variables are therefore directly connected to the twin indicator introduced above. In combination with Eq. (11) we can directly see that the elastic energy becomes quadratic in the spin variables, which is essential for the mapping of

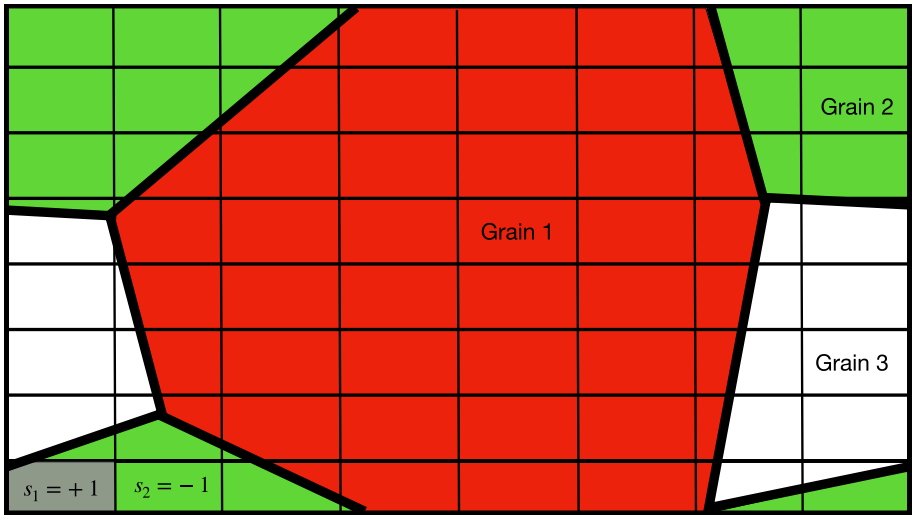

Fig. 2 Illustration of the discretization of the computational domain. The entire sample consists of grains, visualized through different colours. The grains affect the orientation of the crystal and the transformation strain tensor, see Sect. 3.4. The system itself is discretized by domains, which should be significantly smaller than the used grains size (here we use rectangular or quadratic domains; in case that a domain contains part of more than one grain, we use a unique assignment to the grain with the largest volume fraction). Each domain has an assigned spin variable s_i, where $s_i = -1$ means that the domain is in the original state, whereas $s_i = +1$ means that it is in the transformed state, as illustrated in the lower left corner. Through the transformation strain induced internal stresses interactions between the spins arise due to elastic coherency strains, leading in particular to spin-spin interactions J_{ij}. The linear couplings h_i arise in particular through the application of externally applied strains.

the problem to the quantum annealer. In analogy to the previous work [6–8], the elastic energy can then be exactly expressed as Ising Hamiltonian in the framework of linear elasticity,

$$E = \sum_i h_i s_i + \sum_{i<j} J_{ij} s_i s_j + E_0. \tag{12}$$

In other words, for a given microstructure (i.e., knowledge of the spin states of all domains), the elastic energy consists of terms which are linear in the spin value plus additionally pairwise spin-spin interactions between the domains only. The interactions between domains are long-ranged, and therefore the ground state of such a spin glass Hamiltonian is nontrivial. It turns out that the interaction coefficients have to be calculated with very high accuracy to obtain the correct equilibrium microstructure. In particular, the introduction of a cutoff for the range of the interactions is not valid. For details of the formalism and the approach to calculate the Ising coefficients E_0, h_i and J_{ij}, we refer to the supplemental material and [6–8]. To run the QA calculations, we use the D-Wave Quantum Annealer Advantage$^{\mathrm{TM}}$ system.

For smaller systems, typically up to the order of 100 spins, the energy can be minimized using quantum annealing alone in a reliable way, and the default embedding turns out to deliver robust results. To ensure the correct identification of the ground state, we repeat the computation several times. For small systems, as reported in Sects. 3.2 and 3.3, chain breaks typically do not appear and only play a role for larger number of spins. For polycrystalline simulations in Sect. 3.4, which require thousands of spins, we use hybrid approaches, which combine quantum annealing with conventional minimization algorithms. This functionality is directly provided by D-Wave through their hybrid solver. The scaling of the algorithms, both for pure QA and hybrid minimization, has

been investigated for the related problem of martensitic transformations in [6], which also induce long range spin-spin interactions, showing the strong performance of the QA, as compared to brute force and probabilistic approaches. For comparisons of the QA performance with state-of-the-art classical solvers, digital annealing and gate-based approaches such as the QAOA, we refer to existing benchmarking studies [55–58].

2.4 Molecular dynamics

For comparison, the deformation behavior is investigated using Molecular Dynamics (MD) via the Large-scale Atomic/Molecular Massively Parallel Simulator (LAMMPS) [59]. Analysis and visualization are carried out with the support of OVITO [60] and Gnuplot [61]. Bcc crystal structures are simulated at their equilibrium lattice constants. The empirical embedded atom model (EAM) inter-atomic potential for lithium developed by Nichol and Ackland [62] is used. An earlier comparison of lithium interatomic potentials indicated good performance of the Nichol–Ackland EAM potential [63]. As the benchmark with MD simulations is here rather on a qualitative level, the choice of the potential is not critical.

For free-standing Li nanopillars, single crystals with the orientation [001] parallel to the loading direction are tested in tension. The specific orientations are $[001] \parallel z$, $[100] \parallel x$ and $[010] \parallel y$. Simulations are run with periodic boundary conditions in z direction (long, central axis of the nanopillar and loading direction), but non-periodic in x and y direction, with free boundary conditions at the mantle of the pillar. The specimens are first temperature equilibrated at 300 K using an NVT ensemble for 40,000 time steps and then strained with a fixed strain rate of 10^8 s^{-1} along the z direction using also an NVT ensemble at 300 K.

A full analysis on, e.g., the structural information of the potential, size effects, strain rate effects, sensitivity and repeatability of the simulations, as well as a comprehensive review on lithium mechanics can be found in [36].

3 Results and discussions

3.1 Twin interface orientations

The above formulation allows for a continuum description of twinned structures, as the orientation states of their twin components differ only by the eigenstrain expressions, with a coherent interface in between them. To understand the role of the elastic energy on the twin interface, we set up an array of straight lamellae using a periodic setup, as sketched in Fig. 3a. For determining the lowest energy configuration with a planar interface between these regions, it is sufficient to calculate the elastic energy in a system consisting of two equally sized layers, and vary their crystallographic orientation. The following results are obtained from an isotropic elasticity calculation using a Poisson ratio of $\nu = 1/4$.

Figure 3a sketches the setup of the calculations, where the twin components have the same volume fractions. Both parts of the crystal initiate from the same crystallographic orientation, and the twin eigenstrain shear tensor is applied to half of the setup. With the use of periodic boundary conditions, the system consists of a stripe pattern with alternating sheared (transformed) and not sheared (original) regions, i.e., a twinned crystal with lamellar twin components. Then, the entire crystal structure is rotated (rotation axis $[1\bar{1}0]$) while keeping the interface vertically, so that the energy of different

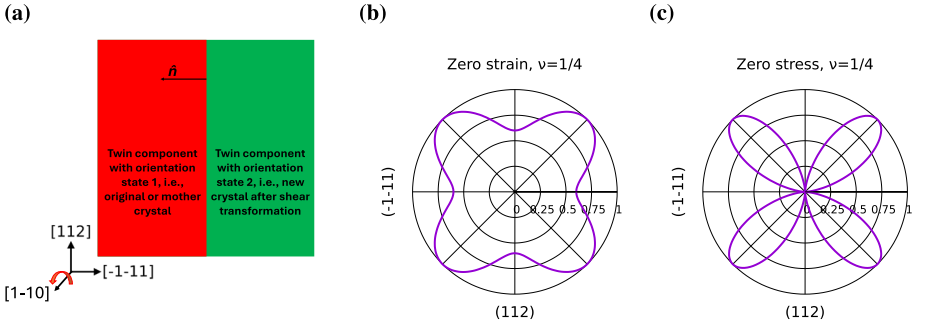

Fig. 3 (**a**) Sketch of the twinned geometry, using periodic boundary conditions. The local coordinate system indicates the rotation of the crystal, $\hat{n}$ is the interface normal direction, as used in the subsequent polar plots. (**b**) Polar plot of the normalized elastic bulk energy for vanishing external strain, $\langle \epsilon_{ij} \rangle = 0$, with indicated normal directions of the twin interface. (**c**) The same for zero average stress, $\langle \sigma_{ij} \rangle = 0$. In both cases the Poisson ratio is chosen as $\nu = 1/4$.

interfaces can be calculated. We note that in the absence of external stresses or strains this approach is equivalent to keeping the lattice orientations fixed, but rotating the interface normal of the dividing plane between the original and shear regions.

Figure 3b and c show the elastic energy of the system for both zero average strain and stress boundary conditions in polar representation. In the polar plots, the normal orientation of the interface is shown relative to the lattice orientation, as defined in Fig. 3a. The energy is always scaled to the maximum value, which depends on the chosen boundary condition. Obviously, these two cases differ significantly, as for the stress free case the elastic energy is cusped, as further discussed below. In both cases, the energy reaches its minimum in particular for (112) interface orientations, hence the continuum description – which is ignorant of the underlying crystallography – correctly captures the expectation that (112) is a favorable interface orientation. However, a second spurious preferred interface orientation appears, $(\bar{1}\bar{1}1)$, which is not a twin interface from a crystallographic perspective. We must emphasize that up to this point only bulk elasticity for coherent interfaces is taken into account, but other possible energy contributions, such as interfacial energies, are neglected so far. As a consequence, pure elasticity is not sufficient to select the desired (112) orientation, as rotations of the crystal by 90° also lead to such preferred orientations.

We point out that this effect, which may seem at a first glance as an artifact of the chosen description, should appear similarly in phase-field models of twin formation, which use a corresponding elastic energy based description using eigenstrains for the twin formation [37, 40]. For instance, in [40], an anisotropic interfacial energy, which is much lower for the twin interface than for other grain boundaries, is used to favor the desired interface. Therefore, also here it is important to include an interfacial contribution which gives preference to the expected twin interface.

From the bulk elastic perspective alone, for the zero stress boundary conditions, internal coherency stresses do not arise if the interfaces are oriented such that a pure shear arises in the tranformed twin components (as expressed through the eigenstrain tensor (2)), as then the original twin component is not deformed. This is the case if the interface between the two components coincides with either the (112) or $(\bar{1}\bar{1}1)$ planes. For other orientations tangential stresses appear at the interface due to the rotation of the eigenstrain tensor, and then the elastic energy is increased. We note that in our description, for both zero external strain and zero external stress cases, the elastic energy of a single,

non-twinned crystal is zero, and twinning appears only under the presence of an external load.

3.2 Prediction of twin formation via quantum annealing

So far, we have used a given twinned microstructure with fixed sizes of the original and transformed twin components to investigate the agreement of the continuum description with crystallographic expectations concerning the selection of the preferred twin interface orientation. In this section, we add the quantum annealing framework for selecting the distribution of twin components based on the global minimization of the elastic energy. Therefore, we discretize the studied sample into small "domains", to which we assign one Ising spin variable $s_i = \pm 1$ each. We use here the convention that $s_i = -1$ and $s_i = +1$ correspond to the original and transformed orientation state of each domain, respectively. By choosing a sufficiently fine domain decomposition, arbitrary arrangements of twin components can be described. According to the formalism which describes the elastic state from a continuum perspective with coherent interfaces between the domains with different eigenstrain, the mechanically equilibrated (in the sense of Equation (10)) elastic energy can be written as Ising Hamiltonian, see Equation (12). This transformation has been derived in [6–8]. The Ising coefficients can be computed through a series of elastic calculations, where only one or two domains are in the transformed orientation state. The determination of the microstructure then turns into a discrete global minimization of the Ising Hamiltonian with respect to the spin variables s_i.

We demonstrate the approach using a discretization which is adapted ideally to the symmetries of the twinning, using a description in the coordinate system B', as then small simulations with only a minimum number of domains are sufficient. In particular, the $[1\bar{1}0]$ (y') direction has a vanishing eigenstrain contribution, and the use of a plane strain description is appropriate. A tensile strain $\langle \epsilon_{zz} \rangle$ in $[001]$ (z) direction translates in the rotated frame B' to prescribed average strains of $\langle \epsilon_{x'x'} \rangle = 1/3 \langle \epsilon_{zz} \rangle$, $\langle \epsilon_{x'z'} \rangle = \sqrt{2}/3 \langle \epsilon_{zz} \rangle$ and $\langle \epsilon_{z'z'} \rangle = 2/3 \langle \epsilon_{zz} \rangle$. We note that only the shear component $\langle \epsilon_{x'z'} \rangle$ triggers the formation of twins, as the other components lead to tensile contributions, as expressed through the transformation tensor (2).

Due to the chosen problem adapted coordinate system, one can use a rather coarse domain decomposition, as twin lamellae are expected to form parallel to the coordinate axes. For illustrational purposes, we use the decomposition on 8×8 quadratic domains in the $x'z'$ plane, as shown in Fig. 4. This sequence of figures shows the layer-by-layer growth of the twin, in agreement with the atomistic simulations from [3]. The green regions correspond to the transformed twin components. From the pure bulk elastic perspective, the twin growth must not necessarily happen in a strictly ordered layer-by-layer sense, as it is energetically equivalent to form thicker twin lamellae or several smaller ones, as long as their volume ratio is the same. This effect has been discussed in detail in [8] and again reflects the need of a twin interface energy contribution. The undesired energetic degeneracy of (112) and $(\bar{1}\bar{1}1)$ interfaces from a bulk elastic perspective alone, where the latter interface does not correspond to a twin interface, is cured immediately by the use of an anisotropic interfacial energy between the twin components.

The obtained observations are remarkable, as they differ from time dependent computations using, e.g., crystal plasticity on the growth of twins. In such simulations, the

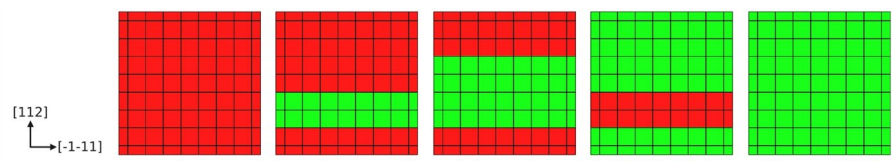

Fig. 4 Twin formation modeled in single crystals using quantum annealing. The horizontal direction corresponds to the $\hat{x}' \parallel [\bar{1}\bar{1}1]$ direction and the vertical direction to the $\hat{z}' \parallel [112]$ orientation. A tensile strain is applied in [001] direction, and periodic boundary conditions are used in $\hat{x}'$ and $\hat{z}'$ direction. In the perpendicular $\hat{y}'$ direction a plane strain situation is assumed. The twin components in transformed orientation state are shown in green. From left to right the applied strains are $\langle \epsilon_{zz} \rangle = 0$; 3/16, 3/8; 9/16; 3/4. For $\langle \epsilon_{zz} \rangle > 3/8$ the transformed twin component becomes the majority phase. We emphasize that the arrangement of the layers is translation invariant in vertical direction, hence the arrangement of the layers can change in between the figures. Notice that the domains are shown in the Lagrangian reference frame, i.e., not showing the actual shear deformation through the twinning. For these simulations, a (weak) anisotropic interfacial contribution is included, as discussed in more details in Sect. 3.3 and at the supplemental material (Figure S1).

orientation of a twin is typically fixed by the initial "nucleus", which grows subsequently in the given direction. In contrast, the QA simulations are independent simulations for each applied external strain, reflecting quasistatic transitions between ground state configurations. Therefore, without the anisotropic interface contribution, lamellae can spontaneously break into smaller ones (with the same volume fraction) or change their orientation by 90° due to energetic degeneracy of the bulk mechanical energy.

In absence of an external strain, $\langle \epsilon_{zz} \rangle = 0$, the entire material is in the original orientation state, but as soon as a tensile strain is applied, twinning occurs, and the volume fraction of transformed twin components increases with strain. In the shown simulations, the growth occurs rather step-wise due to the chosen coarse discretization, but for smaller and more domains, the growth becomes more and more continuous. In the end, we arrive at a volume fraction, which increases linearly above $\langle \epsilon_{zz} \rangle > 0$, until the entire sample has undergone the transformation. Although these finding agree with atomistic simulations of deformation twinning in [3] at a first glance, still discrepancies remain, which are discussed in detail in the following section.

Furthermore, we can understand the twin growth in the present simulations analytically for an infinitely fine domain discretization. In this case, the stress $\sigma_{x'z'}$, induced by the transformation strain (2) remains strictly zero. With the volume fraction v of transformed twin components we have the average eigenstrain $v/2\sqrt{2}$, which has to match the prescribed value $\langle \epsilon_{x'z'} \rangle = \sqrt{2}/3 \langle \epsilon_{zz} \rangle$, therefore leading to

$$v = \frac{4}{3} \langle \epsilon_{zz} \rangle. \tag{13}$$

This prediction is indeed in agreement with the findings in Fig. 4.

3.3 Twin interface energy

It is instructive to qualitatively compare the predictions from the continuum model, as it is developed up to this point, to atomic scale simulations. We use a description which is close to the tensile tests of free standing nanowires and nanopillars using Molecular Dynamics (MD) simulations in [18, 19, 30–33, 36]. Results are shown in Fig. 5, which depicts an exemplary simulation of a tensile test of a bcc lithium single crystal nanopillar with crystallographic directions as $[001] \parallel z$, $[100] \parallel x$ and $[010] \parallel y$. When the specimen is strained along the [001] direction, the pillar forms reflection twins with $(\bar{1}12)$ twin

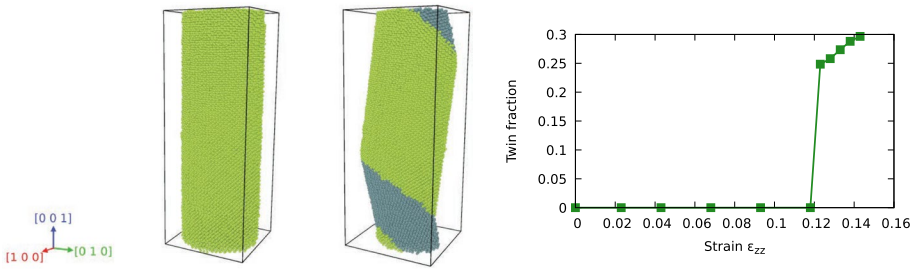

Fig. 5 MD simulation of a lithium single crystal ([001] ∥ z) with 4 nm radius and 20 nm height. Tensile strain is applied along [001]. The original orientation state is colored in light green, while the transformed orientation state is colored in dark green. The polyhedral template matching and grain segmentation filters from Ovito are used [60, 64]. The snapshots are respectively from strains 0.118 (right before main twinning event), 0.123 (right after main twinning event).

interfaces and common $[\bar{1}1\bar{1}]$ axes. Upon twinning, the crystal only deforms in the (110) plane, in agreement with the discussion in Sect. 2.1. There is no deformation along [110]. Contrary to the continuum prediction, as expressed through Equation (13), the twinning requires a minimum strain to appear in the sense of a nucleation event due to the need to overcome a Peierls-Nabarro barrier for the formation of a stacking fault. Only after this nucleation event, the twin fraction increases linearly with strain, which is the result of a layer-by-layer reorientation of the original crystal, similar to discussions in [23, 30]. The discrepancy between the MD and QA behaviors can be resolved through an interfacial energy in the continuum description. Additionally, it prevents splitting of twins into smaller lamellae, which have the same bulk elastic energy as a single bigger lamella. Most importantly, as discussed above, the anisotropic interfacial grain boundary energy is needed to suppress the formation of unexpected $(\bar{1}\bar{1}1)$ grain boundary orientations.

All effects can be overcome through the consideration of nearest neighbor spin-spin interactions for an interfacial energy contribution, as demonstrated in [8]. In fact, different spin states in neighboring domains indicate the presence of a twin interface in between them, to which we attribute an interfacial energy σ. We use here a weakly anisotropic interfacial energy, favoring the crystallographically expected (112) twin boundaries. The actual amount of anisotropy is not significant at this point, as it is sufficient to simply break the symmetry between the formerly energetically equivalent configurations, see Fig. 3. To this end, we add to the Ising Hamiltonian an additional pair interaction term of the type $-s_i s_j \sigma(\theta) A_{ij}/2$ for nearest neighbors i and j. The reason for this term is that $(1 - s_i s_j)/2$ equals one for distinct orientation states $s_i = -s_j$, whereas it vanishes inside the bulk phases. Additionally, A_{ij} is the area of the common interface of these two domains (interface length in two dimensions), and $\sigma(\theta)$ represents the anisotropic interfacial energy, with θ being the local interface normal. More details are available at the supplemental material (Figure S1).

As confirmed in Fig. 4, we find that the addition of a small interfacial energy $\sigma > 0$ is also sufficient to prevent the splitting into micro-lamellae, which is unfavorable from the perspective of interfacial energy. To further investigate the influence of the twin interface energy on the onset of deformation twinning, we performed a series of simulations similar to Fig. 4, but with a finer discretization in the [112] direction, using 1×32 rectangular domains. Figure 6 shows the volume fraction of transformed twin components as function of the applied tensile strain in z direction. In agreement with the preceding investigations and Equation (13), the volume fraction of transformed twin components

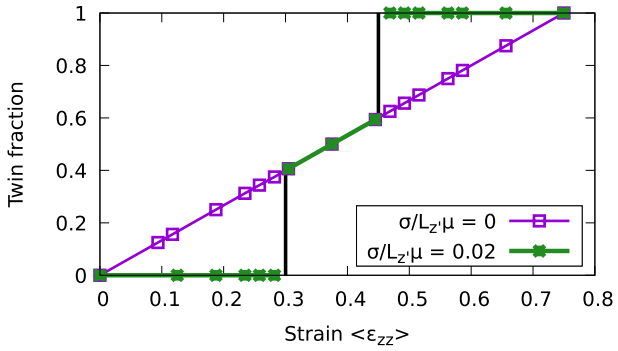

Fig. 6 Volume fraction of transformed twin lamellae as function of the applied tensile strain on single crystals. Without interfacial energy the twin formation starts at zero strain, and the volume fraction of transformed twin components increases linearly up to the upper limit $\langle \epsilon_{zz} \rangle = 3/4$, where the entire sample is transformed. With interfacial energy, first a nucleation barrier has to be overcome, both from the original and fully transformed side. The QA calculated transitions of twin formation agree with the analytical predictions (16) and (17), as marked by the vertical black lines. In these QA simulations, a decomposition into 1×32 grains is used in a quadratic system with edge length $L_{x'} = L_{z'}$, with the axes orientations as in Fig. 4. The Poisson ratio is chosen as $\nu = 1/4$.

increases linearly with the applied strain in the absence of interfacial energy. With grain boundary energy, it requires a finite activation barrier to form the twin. Notice that this behavior happens symmetrically coming from the fully transformed state, as then for the appearance of domains with the original orientation state again a nucleation barrier has to be overcome. In general, the twin formation becomes hysteretic due to this new energy term. As discussed, the quantum annealing finds the absolute minimum of the energy landscape, it does not follow metastable branches. However, close to the transition the QA does not always find the true ground states directly, and the number of required readout repetitions increases in this regime. Overall, the behavior now agrees with the MD simulations of twinning at nanopillars (Fig. 5), where first a strain needs to be built up, before the release of this strain is sufficient to overcome the nucleation barrier of the twin interface energy.

The behavior in the QA simulations can also be understood analytically. From the elastic energy (8) in the system only the shear related part is relevant here, as due to the transformation strain in the frame B' the diagonal parts of the strain tensor are not affected. Below the threshold of twinning, the uniform shear leads to a free energy contribution

$$F_{\text{shear}} = 2\mu \langle \epsilon_{x'z'} \rangle^2 L_{x'} L_{z'}, \tag{14}$$

per length in y' direction, where $L_{x'}$ and $L_{z'}$ are the system lengths in the respective directions. From the strain rotation we have $\langle \epsilon_{x'z'} \rangle = \sqrt{2} \langle \epsilon_{zz} \rangle / 3$. Beyond the onset of twinning, the shear strain is fully compensated by the eigenstrain in a lamella of suitable width, as discussed in the previous section. Therefore, here only the interfacial energy (per length in y' direction) remains, which reads

$$F_s = 2 L_{x'} \sigma. \tag{15}$$

Therefore, the twin will nucleate above the threshold strain

$$\langle \epsilon_{zz}^{\text{crit, 1}} \rangle = \frac{3\sqrt{\sigma}}{\sqrt{2 L_{z'} \mu}} \tag{16}$$

to minimize the energy. This threshold is marked as vertical line in Fig. 6 and coincides with the annealer results.

An analogous analysis can be carried out in the high strain result, where a twin component with original orientation state has to nucleate. In this case the threshold strain reads

$$\langle \epsilon_{zz}^{\mathrm{crit},\ 2} \rangle = -3\sqrt{\frac{\sigma}{2L_{z'}\mu}} + \frac{3}{4}, \tag{17}$$

which is also marked in the plot. Again, the QA results agree with this prediction, which are in line with the MD results. Furthermore, we note that the threshold strain for twin formation, $\langle \epsilon_{zz}^{\mathrm{crit}} \rangle \sim 1/\sqrt{L_{z'}}$, due to the interplay of interfacial and bulk mechanical effects, is analogous to the well-known Hall-Petch equation, which states a relationship of yield strength with grain size to the power of $-1/2$ [65, 66]. In fact, for most twinning cases the Hall-Petch relation is indeed obeyed, but with a higher slope than for slip [17].

3.4 Twinning in polycrystals

With the investigations of planar twins on single crystals and the understanding of twin interface energetics from the preceding sections, we are now equipped to perform larger scale simulations of polycrystals.

In polycrystals, it is difficult to predict which arrangement of twin components leads to a global minimum of the mechanical and interfacial energy. Although it is possible to perform also dynamical atomistic or continuum simulations, they can get stuck in local energetic minima, and the relaxation to the ground state can be prohibited or take a long time. Here the QA approach can be a useful way to directly find the equilibrium state.

Also at the QA level, a larger number of domains is required to properly discretize the polycrystalline system as compared to the small simulations shown before. The drawback of this step is that more domain-domain interactions for computing the Ising coefficients are required, and the overall computation time increases. As a consequence, for computational reasons, the number of domains should be not too large. However, one has to keep in mind that periodic boundary conditions can affect the selection of the twins. With planar twins, the periodicity does not have an effect, as twin lamellae appear parallel or perpendicular to the axis (as shown in Fig. 4). On the other hand, if the choice of coordinate system leads to the appearance of inclined twins (as shown in Fig. 5), the periodicity, in combination with the externally applied load, can instead enforce them to appear at other orientations rather than (112). We note that this effect similarly appears in other simulations, is not specific to the present model and has been discussed before in a similar context in [6].

In the QA framework, we can independently vary the eigenstrain in each domain to represent different grain rotations. A technical difference between these polycrystalline simulations and the ones performed in [7] is that in the latter each grain was connected to one spin, while here an additional subdivision of the grains into domains is necessary, as the transformed twin components typically occupy only a small amount of entire grains, and therefore multiple spins per grain are used. In the example shown in Fig. 7 we use a setup consisting of five grains with different, randomly chosen orientations, subjected to periodic boundary conditions. The grains are considered as static and a grain boundary energy contribution is not included in the description (contrary to the

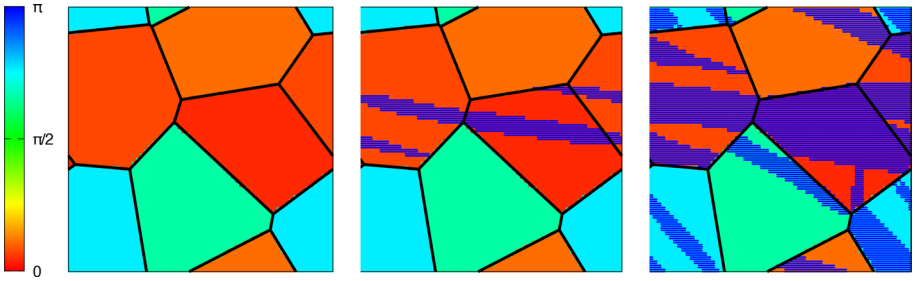

Fig. 7 Deformation twinning in a polycrystal consisting of five grains. Here, the coordinate system is given by the basis set B', i.e., the horizontal axis corresponds to the $\hat{x}' \parallel [\bar{1}\bar{1}1]$ axis and the vertical axis to the $\hat{z}' \parallel [112]$ axis. Relative to these axis, the grains are rotated in the $x'z'$ plane in anti-clockwise direction, as indicated by the color coding. A tensile strain is applied in [001] direction, which is $\langle \epsilon_{zz} \rangle = 0$ in the left panel, $\langle \epsilon_{zz} \rangle = 0.1$ in the middle panel, and $\langle \epsilon_{zz} \rangle = 0.3$ in the right panel. The blue shading indicates the domains in transformed orientation state, i.e., the domains with Ising spin $+1$. Additionally to the tesselation by grains, the periodic system with plane strain boundary conditions is divided into 64×64 domains in the sense of the preceding discussion, hence altogether 4096 Ising spins are used. As third discretization level, a uniform mesh of size 2048×2048 is used for the Fourier transformation based self and domain interaction energy calculations, using $\nu = 1/4$. The simulation results include apart from elastic energy also a weak, anisotropic interfacial energy to favor twinning on the (112) plane (see supplemental material Figures S1 and S2).

twin interface energy discussed above). Each grain contains approximately 800 domains, and the grain orientation is shown as color code. The reference system is chosen to coincide with the preceding computations which used the basis B'. So, for a grain with orientation $\theta = 0$ (shown in red in the figure) the horizontal axis corresponds to the lattice orientation $[\bar{1}\bar{1}1]$ and the vertical axis to [112]. As before, a tensile strain is applied in [001] direction. Results for different applied external strains are shown in Fig. 7.

Although the overall behavior is significantly more complex than in the single crystals cases studied above, there are a few general conclusions which can be drawn:

i) Twinning happens preferentially in grains without rotation, similar to Fig. 3, as the driving force for the transformation is maximized. Therefore, most of the red grains are twinned. Also, the twin orientations are close to the predictions.

ii) In the light blue grain, which is rotated by around $3\pi/4$, also the twin interfaces are rotated accordingly, as the (112) twin boundaries are energetically favorable. Still, this does does not exclude the formation of transformed domains without a twin interface, if strongly favored by bulk relaxation (orange grain). We note that the anisotropic interfacial energy contribution in the example is rather small (see supplemental material, specifically Figure S2, for details).

iii) Twinning usually stops at high angle grain boundaries (interfaces between green and red or blue and red grains in Fig. 7), whereas low angle boundaries (interfaces between red and red grains) are permeable to twin progression.

iv) Twin domains can appear close to the grain boundaries, leading to deviations from the crystallographically expected orientation due to locally nontrivial deformation states. This is the case in the green colored grain.

v) Qualitatively, the microstructure is similar to those observed via optical microscopy, electron microscopy and EBSD characterization in experiments with polycrystalline bcc metals (see, e.g., [67, 68]) and close-packed structures (see, e.g., [24, 69]) which deform primarily by twinning. Important features regarding twin transmission through grain boundaries and formation of lamellar twins can be identified in both experimental and our pictures.

vi) The characteristic lenticular shape of deformation twins is partly observed in the present simulations as a consequence of minimization of mechanical energy. This effect becomes screened if a twin traverses the entire sample, as then the strain is reduced homogeneously.

vii) Interfacial energy contributions lead to the appearance of a nucleation barrier, and therefore promotes less, but wider twin components with a high release of mechanical energy, which are properly aligned to the external mechanical load.

Overall, the presented continuum approach for describing deformation twins has the potential to support simulations of this deformation mechanism, complementing atomistic approaches, like Molecular Statics and Dynamics, kinetic Monte-Carlo approaches [70], as well as continuum methods, like Crystal Plasticity based Finite Element Simulations. The detailed interplay between microstructure, the crystallography of twinning and complex mechanical effects will be elucidated in future investigations.

4 Conclusions

Modeling deformation mechanisms and microstructure formation is critical for many materials science applications, and efficient simulation approaches to predict equilibrium microstructures in large systems are highly desired. Mainly bcc metals remain intricate to model due to their complex deformation behavior, while their importance in, e.g., battery technologies, grows consistently. In this work, we extend insights of deformation twinning in bcc metals from an atomistic level to a continuum scale using quantum annealing (QA). We have developed a framework to bridge the scales by bringing crystallography and theoretical knowledge into a QA formulation and simulate deformation twinning in large systems. We have compared the continuum descriptions to MD simulations of lithium due to its relevance for battery research. Still, the approach is not material-specific and it should be applicable in a similar way to other systems in which twinning is a relevant deformation mechanism, including other crystal structures like fcc, and we will investigate these aspects in the future. Also, the external load is not limited to tensile strains, and arbitrary stress states, including shear contributions, can be captured in an analogous fashion.

Building on an existing QA framework that captures shear transformations via an Ising model, we have added crystallographic knowledge specific to bcc deformation twinning and twin interface energetics. This enables accurate simulations of deformation twinning for given external mechanical load. In single crystals, the QA predictions agree conceptionally with MD simulation results of deformation twinning. In polycrystals, the QA model makes it feasible to scale up the predictions to larger and more complex microstructures, which are closer to reality, delivering deformation twin arrangements comparable to experimental observations. As such, the QA complements available modeling techniques by outputting directly the equilibrium ground structure of large systems extremely fast, while classic techniques, such as MD, FEM, Monte Carlo simulations and phase-field modeling, typically follow the temporal evolution and can suffer from slow convergence. In particular, MD simulations typically require unrealistically high strain rates due to time constraints, while the QA approach represents the opposite with an infinitely slow straining, i.e., a quasistatic process.

Altogether, this novel framework shows that the use of quantum annealing is a promising approach for obtaining ground-state configurations in mechanically strained

systems, which experience stress relaxation through deformation twinning. A particular advantage is that the time consuming computations of the mutual domain interactions need to be calculated only once, whereas changes in the externally applied stress or strain can be treated analytically. The QA simulations are very fast, with actual computation times in the microsecond range for pure QA simulations, and runtimes at the order of seconds for larger hybrid simulations. In addition, variations of the interfacial energy are treated on the annealer level, and therefore these calculations are very fast. At the same time, one should be aware of potential limitations of the approach in the present form, including the assumption of homogeneous and linear elasticity to preserve superposition and restrict the effective interactions between the domains to pairwise terms, which can be handled with the quantum annealer. Deviations from these assumptions can lead to many-body terms, which could possibly be treated through perturbation approaches. Additionally, the complementary concept of the approach to go directly to equilibrium states, as compared to time evolutions described, e.g., by MD or phase field approaches, has to be kept in mind, as rate dependent effects, temperature, plastic slip–twin interactions or non-equilibrium phenomena are intentionally not covered by the presented QA approach.

We point out that the present energy minimization based description of deformation twinning, which is complementary to stress based considerations, is a valuable concept also independent of quantum computing implementation. In fact, digital annealears, which are also based on Ising Hamiltonians, are an alternative to quantum annealing and could instead be used. Moreover, if such dedicated hardware options are not available, conventional discrete optimization methods, probably tuned to the particular problem for performance optimization, could still be used with the same workflow. Still, the quantum annealing, as part of the rapidly developing field of quantum computing, has the potential to significantly exceed the capabilities of existing computational approaches in the future, possibly also for finite temperatures [71]. The presented work is therefore a step towards exploiting this promising technology for materials science applications.

Potentially, future model extensions could include multiple grain variants and other mechanical loadings, which can occur, e.g., during tribological applications, paving the way for realistic, fast and accurate predictions of microstructures of technologically critical materials.

Supplementary Information

The online version contains supplementary material available at https://doi.org/10.1007/s43939-026-00612-8.

Supplementary file 1

Acknowledgements

The authors gratefully acknowledge the computing time granted by the JARA Vergabegremium and provided on the JARA Partition part of the supercomputer JURECA [72] at Forschungszentrum Jülich under project acronym *hetbat* and the Jülich Supercomputing Centre (https://www.fz-juelich.de/ias/jsc) by providing computing time on the D-Wave Advantage™ System JUPSI through the Jülich UNified Infrastructure for Quantum computing (JUNIQ).

Author contributions

L. C. P. S., A.D., D. G., Y. L. B., C. G. and R. S. developed the model, L. C. P. S. and R. S. conducted the simulations, D. G. performed the crystallographic analysis. All authors contributed to the discussions, read, reviewed and contributed to the writing of the manuscript.

Funding
Open Access funding enabled and organized by Projekt DEAL. This work was funded by the German Federal Ministry of Education and Research (BMBF) via the project ALANO (grant no. 13XP0396B) and the Helmholtz Initiative and Networking Fund (project KA-QUS-03 – QT-Batt). Open access was funded by the Deutsche Forschungsgemeinschaft (DFG, German Research Foundation) - 491111487.

Data availability
The datasets generated during and analysed during the current study are available from the corresponding author on reasonable request.

Declarations

Ethics approval and consent to participate
Not applicable.

Consent for publication
Not applicable.

Competing interests
The authors declare no competing interests.

Received: 17 December 2025 / Accepted: 2 March 2026
Published online: 26 March 2026

References

1. Shim J, Lee E-K, Lee YJ, Nieminen RM. Density-functional calculations of defect formation energies using supercell methods: defects in diamond. Phys Rev B. 2005;71:035206.
2. de Van Walle CG, Janotti A. Advances in electronic structure methods for defects and impurities in solids. Physica Status Solidi (b). 2011;248:19–27.
3. Gröger R, Holzer J, Kruml T. Twinning and antitwinning in body-centered cubic metals. Comput Mater Sci. 2023. https://doi.org/10.1016/j.commatsci.2022.111874.
4. Kotrechko SA, Filatov AV, Ovsjannikov AV. Molecular dynamics simulation of deformation and failure of nanocrystals of bcc metals. Theor Appl Fract Mech. 2006;45:92–9.
5. Wong SL, Madivala M, Prahl U, Roters F, Raabe D. A crystal plasticity model for twinning- and transformation-induced plasticity. Acta Mater. 2016;118:140–51.
6. Sandt R, Bouar YL, Spatschek R. Quantum annealing for microstructure equilibration with long-range elastic interactions. Sci Rep. 2023. https://doi.org/10.1038/s41598-023-33232-w.
7. dos Santos LCP, et al. Elastic energy driven multivariant selection in martensites via quantum annealing. Phys Rev Res. 2024;6:023076.
8. Sandt R, Le Bouar Y, Spatschek R. Microstructure equilibration with consideration of elastic and interfacial interactions via quantum annealing with application to the solid electrolyte LLZO. Phys Rev Res. 2024;6:033047.
9. Xu Z, Shang W, Kim S, Lee E, Luo T. Quantum annealing-assisted lattice optimization. NPJ Comput Mater. 2025;11:4.
10. Nguyen V-D, Wu L, Remacle F, Noels L. A quantum annealing-sequential quadratic programming assisted finite element simulation for non-linear and history-dependent mechanical problems. Eur J Mech A-Solids. 2024;105:105254.
11. Sukulthanasorn N, et al. A novel design update framework for topology optimization with quantum annealing: application to truss and continuum structures. Comput Methods Appl Mech Eng. 2025;437:117746.
12. Binninger T, Ting Y-Y, Kowalski PM, Eikerling MH. Optimization of ionic configurations in battery materials by quantum annealing. Phys Rev B. 2024;110:L180202.
13. Hatakeyama-Sato K, Kashikawa T, Kimura K, Oyaizu K. Tackling the challenge of a huge materials science search space with quantum-inspired annealing. Adv Intell Syst. 2021;3:2000209.
14. Sampei H, et al. Quantum annealing boosts prediction of multimolecular adsorption on solid surfaces avoiding combinatorial explosion. JACS Au. 2023;3(4):991–6.
15. Binninger T, et al. Simulating charging characteristics of lithium iron phosphate by electro-ionic optimization on a quantum annealer. Phys Rev B. 2025;112:174118.
16. Kitai K, et al. Designing metamaterials with quantum annealing and factorization machines. Phys Rev Res. 2020;2:013319.
17. Meyers MA, Voehringer O, Lubarda VA. The onset of twinning in metals: a constitutive description. Acta Mater. 2001;49:4025–39.
18. Sainath G, Choudhary BK. Orientation dependent deformation behaviour of BCC iron nanowires. Comput Mater Sci. 2016;111:406–15.
19. Sainath G, Goyal S, Nagesha A. Plasticity through de-twinning in twinned bcc nanowires. Crystals. 2020. https://doi.org/10.3390/cryst10050366.
20. Dezerald L, Rodney D, Clouet E, Ventelon L, Willaime F. Plastic anisotropy and dislocation trajectory in bcc metals. Nat Commun. 2016. https://doi.org/10.1038/ncomms11695.
21. Ojha A, Sehitoglu H, Patriarca L, Maier HJ. Twin nucleation in Fe-based bcc alloys - modeling and experiments. Model Simul Mater Sci Eng. 2014. https://doi.org/10.1088/0965-0393/22/7/075010.
22. Shi Z, Singh CV. Competing twinning mechanisms in body-centered cubic metallic nanowires. Scr Mater. 2016;113:214–7.
23. Li X, Zhang Z, Wang J. Deformation twinning in body-centered cubic metals and alloys. Prog Mater Sci. 2023. https://doi.org/10.1016/j.pmatsci.2023.101160.
24. Anten K, Scholtes B. Formation of macroscopic twin bands and inhomogeneous deformation during cyclic tension-compression loading of the mg-wrought alloy az31. Mater Sci Eng A. 2019;746:217–28.

25. Zhang J, Du S, Ding S. Crystal plasticity finite element modeling of twin band formation and evolution together with the macroscale mechanical responses of hexagonal metals. Mater Sci Eng A. 2022. https://doi.org/10.1016/j.msea.2022.143856.
26. Wang J, Zhang X. Twinning effects on strength and plasticity of metallic materials. MRS Bull. 2016;41:274–81.
27. Mahajan S. Critique of mechanisms of formation of deformation, annealing and growth twins: face-centered cubic metals and alloys. Scr Mater. 2013;68:95–9.
28. Bhadeshia HKDH. *Worked Examples in the Geometry of Crystals* (Institute of Materials, London, 2001), 2nd edn. Updated 2006; available online.
29. Field DP, Bradford LT, Nowell MM, Lillo TM. The role of annealing twins during recrystallization of Cu. Acta Mater. 2007;55:4233–41.
30. Li S, et al. Superelasticity in bcc nanowires by a reversible twinning mechanism. Phys Rev B. 2010;82:205435.
31. Sainath G, Choudhary BK. Twinning to slip transition in ultrathin bcc Fe nanowires. Phys Lett A. 2018;382:1047–51.
32. Veerababu J, Sainath G, Nagesha A. Twin boundary reversibility characteristics in alpha-fe. Mater Today Commun. 2021;29:102970.
33. Zhang RF, Wang J, Beyerlein IJ, Germann TC. Twinning in bcc metals under shock loading: a challenge to empirical potentials. Philos Mag Lett. 2011;91:731–40.
34. Kalnaus S, Dudney NJ, Westover AS, Herbert E, Hackney S. Solid-state batteries: the critical role of mechanics. Science. 2023. https://doi.org/10.1126/science.abg5998.
35. Esmizadeh S, et al. A review on modeling of nucleation and growth of Li dendrites in solid electrolytes. J Energy Storage. 2024;97:112897.
36. dos Santos LCP, Grüner D, Spatschek R. Atomistic modeling of the mechanical properties and deformation behavior of lithium. Modell Simul Mater Sci Eng. 2025;33:075007.
37. Huang B, Yang J, Luo Z, Wang Y, Wang N. Formation of twin boundaries in rapidly solidified metals through deformation twinning. Materials. 2023. https://doi.org/10.3390/ma16134503.
38. Spatschek R, Müller-Gugenberger C, Brener E, Nestler B. Phase field modeling of fracture and stress-induced phase transitions. Phys Rev E. 2007;75:066111.
39. Tourret D, Liu H, LLorca J. Phase-field modeling of microstructure evolution: recent applications, perspectives and challenges. Prog Mater Sci. 2022;123:100810.
40. Heo TW, et al. A phase-field model for deformation twinning. Philos Mag Lett. 2011;91:110–21.
41. Hu S, Henager CH, Chen L. Simulations of stress-induced twinning and de-twinning: a phase field model. Acta Mater. 2010;58:6554–64.
42. Gu Y, Chen L-Q, Heo TW, Sandoval L, Belak J. Phase field model of deformation twinning in tantalum: parameterization via molecular dynamics. Scripta Mater. 2013;68:451–4.
43. Authier A. International tables for crystallography. D. Physical properties of crystals. second online edn. Chichester, West Sussex: Wiley; 2013.
44. Haasen P. Physical metallurgy, vol. 3. 1996.
45. Landau LD, Pitaevskii LP, Lifshitz EM, Kosevich AM. *Theory of Elasticity* (Butterworth-Heinemann, 1986), 3 edn.
46. Khachaturyan AG. Theory of Structural Transformations in Solids. Mineola, New York: Dover Publications Inc; 2008.
47. Finnila AB, Gomez MA, Sebenik C, Stenson C, Doll JD. Quantum annealing: a new method for minimizing multidimensional functions. Chem Phys Lett. 1994;219:343–8.
48. Brooke J, Bitko D, Rosenbaum TF, Aeppli G. Quantum annealing of a disordered magnet. Science. 1999;284:779–81.
49. Kadowaki T, Nishimori H. Quantum annealing in the transverse Ising model. Phys Rev E. 1998;58:5355–63.
50. Morita S, Nishimori H. Mathematical foundation of quantum annealing. J Math Phys. 2008;49:125210.
51. Rajak A, Suzuki S, Dutta A, Chakrabarti BK. Quantum annealing: an overview. Philos Trans R Soc Lond A Math Phys Eng Sci. 2023;381:20210417.
52. Warren RH. Mathematical methods for a quantum annealing computer. Adv Appl Math. 2018;3:82–90.
53. Johnson MW, et al. Quantum annealing with manufactured spins. Nature. 2011;473:194–8.
54. Boixo S, et al. Evidence for quantum annealing with more than one hundred qubits. Nat Phys. 2014;10:218–24.
55. Kim S, et al. Quantum annealing for combinatorial optimization: a benchmarking study. NPJ Quantum Inf. 2025;11:77.
56. Quinton FA, Myhr PAS, Barani M, Granado PCD, Zhang H. Quantum annealing applications, challenges and limitations for optimisation problems compared to classical solvers. Sci Rep. 2025;15:12733.
57. Oshiyama H, Ohzeki M. Benchmark of quantum-inspired heuristic solvers for quadratic unconstrained binary optimization. Sci Rep. 2022;12:2146.
58. Pelofske E, Bärtschi A, Eidenbenz S. Short-depth qaoa circuits and quantum annealing on higher-order ising models. NPJ Quantum Inf. 2024;10:30.
59. Thompson AP, et al. LAMMPS - a flexible simulation tool for particle-based materials modeling at the atomic, meso, and continuum scales. Comput Phys Commun. 2022;271:108171.
60. Stukowski A. Visualization and analysis of atomistic simulation data with OVITO-the open visualization tool. Model Simul Mater Sci Eng. 2010. https://doi.org/10.1088/0965-0393/18/1/015012.
61. Williams T, Kelley C. "many others". Gnuplot 4.6: an interactive plotting program (2013). http://gnuplot.sourceforge.net/.
62. Nichol A, Ackland GJ. Property trends in simple metals: an empirical potential approach. Phys Rev B. 2016;93:184101.
63. Dorrell J, Pártay LB. Pressure-temperature phase diagram of lithium, predicted by embedded atom model potentials. J Phys Chem B. 2020;124:6015–23.
64. Larsen PM, Schmidt S, Schiøtz J. Robust structural identification via polyhedral template matching. Model Simul Mater Sci Eng. 2016;24:055007.
65. Hall EO. The deformation and ageing of mild steel: III. Discussion of results. Proc Phys Soc Lond B. 1951;64:747.
66. Petch NJ. The cleavage strength of polycrystals. J Iron Steel Inst. 1953;174:25–8.
67. Bolling GF, Richman RH. Mechanical twinning of polycrystalline b.c.c. metals. Can Metall Q. 1966;5:143–60.
68. Florando JN, et al. Effect of strain rate and dislocation density on the twinning behavior in tantalum. AIP Adv. 2016;6:045120.
69. Kumar MA, Beyerlein IJ. Local microstructure and micromechanical stress evolution during deformation twinning in hexagonal polycrystals. J Mater Res. 2020;35:217–41.

70. Jagatramka R, Daly M. The competition between deformation twinning and dislocation slip in deformed face-centered cubic metals. JOM. 2022;74:3799–810.
71. Sandt R, Spatschek R. Efficient low temperature Monte Carlo sampling using quantum annealing. Sci Rep. 2023. https://doi.org/10.1038/s41598-023-33828-2.
72. Jülich Supercomputing Centre. JURECA: data centric and booster modules implementing the modular supercomputing architecture at Jülich Supercomputing Centre. Journal of large-scale research facilities JLSRF. 2021. https://doi.org/10.17815/jlsrf-7-182.

Publisher's Note